

**Investigation into the Design of Broadband
Singly-Fed Electromagnetically Coupled Patch
(EMCP) Antenna Elements and Arrays for
Circular Polarisation**

Kwok L. Chung



Faculty of Engineering
University of Technology, Sydney

A Thesis Submitted for the degree of

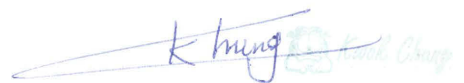
Doctor of Philosophy

November 2004

Statement of Originality

I hereby declare that this thesis has not previously been submitted for a degree nor has it been submitted as part of requirements for a degree except as fully acknowledged within the text.

I also certify that the thesis presents my own work and has been written by me. Any help that I have received in my research work and the preparation of this thesis have been acknowledged. In addition, I certify that all information sources and literature used are indicated in the thesis.



Kwok L. Chung

Dedication

To Fiona, Summi and Michelle,
for their love and patient

Abstract

The rapid development of satellite and wireless communications pose extraordinary demands on broadband circularly polarised (CP) antenna elements and high-performance antenna arrays. The use of high-dielectric-constant materials as the substrate for the driven layer and a low-dielectric-constant material as superstrate for the radiating patch overcomes the conflict between circuit integration and antenna radiation. The aim of the research presented in this thesis is to design and develop high performance singly-fed microstrip patch antennas and arrays for CP applications.

Firstly, we introduce a singly-fed cross-aperture coupled patch antenna and a stacked patch antenna using *high* and *low* dielectric materials known as *Type-F* and *Type-E* elements, respectively. As the physical structure of the *Type-E* element is close to the conventional linearly-polarised electromagnetically coupled patch (LP-EMCP) antennas, we have also denoted it as CP-EMCP antenna. The development of CP-EMCP antennas addresses the drawbacks of the cross-aperture patch antenna. A systematic optimisation method is developed for the design of CP-EMCP elements, at which the mean frequencies of the bandwidths can be adjusted in order to achieve a wide overlaid bandwidth. Secondly, we investigate the effects of perturbation on the

parasitic patch, layer displacements, material tolerances and superstrate thicknesses on the broadband performance as well as the mutual coupling of the CP-EMCP elements. Both our theoretical and experimental results show that the CP-EMCP elements are robust in performance and have a low mutual coupling. When compared to the conventional stacked EMCP antennas and to the reduced surface-wave antenna, the mutual coupling between CP-EMCP elements is lower which allows the use of small element spacings to avoid grating lobes, which therefore make these elements good candidates for high-performance CP arrays.

Following a parametric study on the effect of displacements between stacked patches and the loss consideration of the coplanar feed network printed on high dielectric constant substrates, the *modified Type-E* elements whose parasitic patch have a zero perturbation are developed for the design of high performance CP arrays. The low mutual coupling allows short feed-lines to connect with the spatially offset elements so as to minimise the feed loss. Consequently, it became possible to develop the novel sequentially rotating feed networks which incorporate the modified elements with a small element spacing of $2/3\lambda_0$ for the 4- and 16-element planar antenna arrays. The results indicate that these arrays have high gain, low axial ratio, high antenna efficiency low sidelobe levels, and wide overlaid bandwidth.

Acknowledgements

A thesis like this, contains more than *four* years of research work, does not get written successfully without the faith, advice, support, criticism, and help by people around me, and organisations in supplying or allowing to use many expensive microwave materials and equipment. The following organisations and people are gratefully thanked for their contributions towards this thesis:

The Commonwealth Department of Education, Science and Training, Australia: for the three and half years Australian Postgraduate Award (APA) scholarship, without their financial support this research work would not exist.

Cooperative Research Centre for Satellite Systems (CRCSS): for the 3 years top-up on my APA scholarship, without that I have to do more teaching duties. Thanks also to Dr. Andrew Parfitt, for his technical comment and advice.

ICT Centre at CSIRO: Dr. Trevor Bird, Kieran Greene, Steve Barker, Ken Smart and Li Li, for allowing the use of their indoor chamber for antenna measurements, and their friendly technical support and advice.

Artronic Productions (Australia) Pty. Limited: Ken Wales and his production team, for their kind support and the efficient fabrication of patch antennas.

Rogers® Corporations: for the supply of many free samples of dielectric materials and technical advice.

GIL Technologies: for the supply of dielectric laminates in this research work.

Johnson Components: for the supply of free samples of SMA and SSMA connectors with the technical information.

A/Professor Ananda Mohan Sanagavarapu (A. S. Mohan): for his expert guidance, supervision and his commitment to produce high quality research output. I gratefully acknowledge his advice through all stages of my research, especially with regards to writing of my thesis and the technical papers during the years.

A/Professor Sam Reisenfeld: for his role as my co-supervisor and for providing encouragement and suggestions on my work. Thanks also to his financial support for the travel to the IEEE conferences.

Professors Rod Belcher and Hung T. Nguyen: for their leadership in the Engineering research and development at the UTS, and also for their support in maintaining my full scholarship in the last half-year.

Professor Roman Stere: a respected teacher from the subject of Data Acquisition and Distribution System (DADS), for his sincere help and advice.

Dr. Andrew R. Weily: a typical Oz hard worker and a real researcher, for his enthusiastic help, comments and discussions during my research work.

Dr. John Yong: a good English teacher and a friend of mine, for his proof reading of my writing.

Dr. Henry Zhang, Dr. K. K. Fung and Rosa Tay: for their perspicacious advice, discussions and friendship.

Dr. Venkat Ramaswamy and Dr. Andrew Mears: for giving me teaching duties in the Faculty of Engineering, UTS.

Dr. Heng Chiu, David Tang, Tony Huang, David Smith, S. Kandeepan, Jeffery Tsui, Thung Tran and S. H. Lee: a group of Telecommunications research fellows, who create a great research atmosphere at the Level 20, Building 1 of UTS, for their help, support, comments, criticism and friendship.

Mr. Ray Clout: for his kind of technical support in the Microwave Lab at UTS.

Richard Moor and Ron Smith: for their efficient fabrication of hardware and sound technical support. Their delicate skill made the experimental work so successful. Furthermore, thanks for allowing me to run wild in their Mechanical Workshop while chatting to music.

The Anonymous Reviewers: for their positive comments and suggestions on my IEEE Journal papers.

Finally, but not the least, I would like to express my appreciation to every member of the **Chung's family**: my parents, my brothers, sister, sister-in-law, and my wife for their love and constantly support of my research work.

Publications

Materials presented in the core chapters (Chapter 2 to 5) of this thesis are also available in the following referred/published papers, which are the research output by the candidate during his four-year doctoral candidature at the University of Technology, Sydney.

Chapter 2

- [C2.1] K. L. Chung and A. S. Mohan, "Gain and bandwidth enhancement of a 2.4GHz singly-fed cross-aperture patch antenna", *IEEE Antennas and Propagat., Society Intern Symp.*, Jun 2002, San Antonio. Vol 1, pp. 410-413.
- [C2.2] K. L. Chung and A. S. Mohan, "Techniques to increase gain and impedance bandwidth of a cross-aperture coupled patch antenna", *Microwave and Optical Technology Letters*, Vol. 37, No.4, pp. 283-286, May 2003.

Chapter 3

- [C3.1] K. L. Chung and A. S. Mohan, "A broadband singly-fed electromagnetically coupled patch antenna for circular polarisation", *Proc WARS02, Workshop on the Application of Radio Science*, Sydney, Australia, Feb 2002.
- [C3.2] K. L. Chung and A. S. Mohan, "Singly-fed circularly polarised patch antenna with wide impedance and axial-ratio bandwidth", *2002 IEICE Interim International Symposium on Antennas and Propagation*. Nov, 2002, Yokosuka Research Park, Japan Proc ISAP'02, pp. 275-278.

- [C3.3] K. L. Chung and A. S. Mohan, "A systematic design method to obtain broadband characteristics for singly-fed electromagnetically coupled patch antennas for circular polarisation", *IEEE Transactions on Antennas and Propagation*, Vol. 51, No. 12, pp. 3239-3248, 2003.
- [C3.4] K. L. Chung and A. S. Mohan, "An investigation into an antenna arrays composed of broadband circularly polarised EMCP elements at X-Band". *IEEE Antennas and Propagat., Society Intern Symp.*, Vol 2, pp. 868-871, Jun 2003, Columbus, Ohio.
- [C3.5] K. L. Chung and A. S. Mohan, "Design of stacked circular/quasi-elliptical patch array for broadband CP applications" in Proceedings of *The 6th Intern Symp on Antennas, Propagation and EM Theory*, ISAPE'03, pp. 62-65, Oct 28-Nov 1, 2003, Beijing, CHINA.

Chapter 4

- [C4.1] K. L. Chung and A. S. Mohan, "A broadband electromagnetically coupled patch antenna with robust characteristics against layer misalignments", in Proceedings of *IEEE Canadian Conference on Electrical and Computer Engineering*, 2003. CCECE'03, Vol. 3, pp. 1425-1428.
- [C4.2] K. L. Chung and A. S. Mohan, "A study of mutual coupling between CP electromagnetically coupled patch antennas", in proc. of the *14th International Symposium on Personal, Indoor and Mobile Radio Communications*, PIMRC'03, Vol. 2, pp. 1889-1893, September 7-10, 2003, Beijing, CHINA.
- [C4.3] K. L. Chung and A. S. Mohan, "Mutual coupling between singly-fed circularly polarised stacked patch antennas with various orientations" *Asia-Pacific Microwave Conference 2003*, Vol. 3, pp. 1856-1859, November 4-7, 2003, Seoul, KOREA.
- [C4.4] K. L. Chung and A. S. Mohan, "The effect of offset patch on the broadband characteristics of an electromagnetically coupled patch antennas", *Microwave and Optical Technology Letters*, Vol. 38, No.5, pp. 345-348, Sep 2003.
- [C4.5] K. L. Chung and A. S. Mohan, "Effect of superstrate thickness on the performance of broadband circularly polarised stacked patch antenna". *IEEE Antennas and Propag. Society Intern Symp.*, Vol 1, pp. 687-690, Jun 2004, Monterey, California.

- [C4.6] K. L. Chung and A. S. Mohan, "Effect of dielectric material tolerance on the performance of singly-fed circularly polarised stacked patch antennas". *IEEE Antennas and Propag. Society Intern Symp.*, Vol 1, pp. 479-482, Jun 2004, Monterey, California.
- [C4.7] K. L. Chung and A. S. Mohan, "Experimental study on the performance of circularly polarised stacked patch antenna against layer displacements", *2004 International Symposium on Antennas and Propagation*. Aug, 2004, Sendai, Japan, Proc ISAP'04, pp. 397-400.

Chapter 5

- [C5.1] K. L. Chung and A. S. Mohan, "An investigation into an antenna arrays composed of broadband circularly polarised EMCP elements at X-Band". *IEEE Antennas and Propag. Society Intern Symp.*, Vol 2, pp. 868-871, Jun 2003, Columbus, Ohio.
- [C5.2] K. L. Chung and A. S. Mohan, "Design of stacked circular/quasi-elliptical patch array for broadband CP applications" in Proc. of *The 6th Int. Symp. on Antennas, Propagation and EM Theory*, ISAPE'03, pp. 65-65, Oct 28 - Nov 1, 2003, Beijing, CHINA.
- [C5.3] K. L. Chung and A. S. Mohan, "A circularly polarised stacked electromagnetically coupled patch antenna", *IEEE Transactions on Antennas and Propagation*, Vol. 52, No. 5, pp. 1365-1370, 2004.

Table of Contents

Abstracti

Acknowledgements iii

Publications vi

Table of Contents ix

List of Figures xii

List of Tables xxii

1. Introduction and Overview 1

1.1 CIRCULARLY POLARISED ANTENNAS..... 1

1.2 REVIEW OF SINGLY-FED CIRCULARLY POLARISED PATCH ANTENNAS..... 4

1.3 OVERVIEW ON STACKED AND ELECTROMAGNETICALLY COUPLED PATCH ANTENNAS
.....7

1.4 MOTIVATION FOR THE RESEARCH..... 16

1.5 THE COMMON DESIGN OBJECTIVES OF CIRCULARLY POLARISED PATCH ANTENNAS
.....17

1.6 MEASUREMENT ON CIRCULARLY POLARISED ANTENNAS 20

1.6.1 Axial Ratio and CP Gain Measurements 20

1.6.2 Measurement of Polarisation Patterns 23

1.7 ROAD MAP OF THIS THESIS..... 26

**2. Design of Cross-Aperture Coupled Patch Antenna: Type-F element
..... 27**

2.1 INTRODUCTION 27

2.2 DESIGN OBJECTIVES FOR THE USE OF CROSS-APERTURE..... 29

2.3	TRANSMISSION-LINE MODELLING OF CROSS-APERTURE COUPLED PATCH ANTENNA	30
2.4	PROPOSED ANTENNA GEOMETRY AND ITS DESIGN	36
2.4.1	<i>Selection of Microwave Laminates for the Dielectric Layers</i>	36
2.4.2	<i>Estimation of Patch Sizes and Their Perturbations</i>	38
2.5	ANTENNA PERFORMANCE AND COMPARISON	46
2.6	A PARAMETRIC STUDY	49
2.6.1	<i>The Effect on the Sizes of Upper-Patch.....</i>	49
2.6.2	<i>The Effect on the Sizes of Cross-Aperture.....</i>	52
2.7	DISCUSSION	54
3.	Design of Broadband CP Stacked Electromagnetically Coupled Patch Antennas: Type-E element and its variants	55
3.1	INTRODUCTION	55
3.2	A GENERALISED DESIGN AND TUNING METHOD	57
3.2.1	<i>CP-EMCP Antenna Geometry</i>	57
3.2.2	<i>Selection of Dielectric Materials.....</i>	59
3.2.3	<i>Systematic Design and Tuning Strategy.....</i>	61
3.3	THE THREE DESIGN EXAMPLES.....	67
3.3.1	<i>A Design Example at C-band.....</i>	67
3.3.2	<i>A Theoretical Design at Ku-band.....</i>	77
3.3.3	<i>Another CP-EMCP Element Design at S-band.....</i>	82
3.4	MODIFICATION OF TYPE-E ELEMENTS FOR SEQUENTIAL ROTATION	87
3.4.1	<i>The reasons why it needs modification</i>	87
3.4.2	<i>The modification 1: parasitic patch with zero perturbation</i>	88
3.4.3	<i>The modification 2: circular patch stacked onto a quasi-ellipse</i>	92
3.5	DISCUSSION	97
4.	Effects of Layer Displacements, Mutual Coupling and Material Tolerances on Broadband Characteristics	99
4.1	INTRODUCTION	99
4.2	THE BROADBAND CHARACTERISTICS AGAINST LAYER DISPLACEMENTS	100
4.2.1	<i>An Experimental Investigation on a LP-EMCP Element</i>	101
4.2.2	<i>An Experimental Investigation on a CP-EMCP Element.....</i>	108
4.2.3	<i>The Angular Displacement on Two CP-EMCP Elements</i>	115
4.3	THE EFFECT OF DIELECTRIC MATERIAL TOLERANCES	122
4.3.1	<i>Tolerance Effects on the Type-E Element</i>	123
4.3.2	<i>Tolerance Effects on the Modified Type-E Element.....</i>	126

4.4	MUTUAL COUPLING BETWEEN CP-EMCP ANTENNAS	130
4.4.1	<i>Comparisons in Spatial Domain at Centre Frequency</i>	135
4.4.2	<i>Mutual Coupling of CP-EMCP Elements in Frequency Domain</i>	145
4.4.3	<i>Effect of Superstrate Thickness on Mutual Coupling</i>	152
4.4.4	<i>Mutual Coupling with Elements Orientations</i>	158
4.4.5	<i>Mutual Coupling versus Relative Orientations</i>	165
4.5	DISCUSSION	168
5.	Design of High-Performance Circularly Polarised Antenna Arrays	171
5.1	INTRODUCTION	171
5.2	SEQUENTIALLY ROTATED ARRAY USING CP ELEMENTS	173
5.2.1	<i>The Basic Design Principles by Teshirogi and Hall</i>	174
5.2.2	<i>The Polarisation Stability Factor by Kraft</i>	177
5.2.3	<i>A Supplementary Rule</i>	182
5.3	DESIGN OF HIGH-PERFORMANCE CIRCULARLY POLARISED ARRAYS	187
5.3.1	<i>Loss Consideration in High-Dielectric-Constant Substrates</i>	187
5.3.2	<i>Design of Coplanar Feed network for 2x2 subarrays</i>	194
5.3.3	<i>The High Performance 2x2 Sequential Rotation Arrays</i>	200
5.3.4	<i>Design of 4x4 Rotated Array with a Low-Loss Feed Network</i>	209
5.4	DISCUSSION	218
6.	Conclusions and Future Work	220
6.1	MAJOR CONTRIBUTIONS OF THIS THESIS	220
6.1.1	<i>Introduction</i>	220
6.1.2	<i>The Major Contributions</i>	221
6.2	CONCLUSIONS ON THE CORE CHAPTERS	224
6.2.1	<i>Cross-Aperture Coupled Patch Antenna</i>	224
6.2.2	<i>Circularly Polarised Stacked EMCP Antennas</i>	225
6.2.3	<i>Robust Characteristics and Mutual Coupling of CP-EMCP Antennas</i>	226
6.2.4	<i>High-Performance Circularly Polarised Arrays</i>	229
6.3	SUGGESTED IMPROVEMENTS AND FUTURE WORK.....	230
	References	232
	Appendix	245

List of Figures

Figure 1.1	A direct approach to generate circular polarisation from a square patch antenna using the orthogonal (dual) feeds: (a) by a reactive splitter; (b) by an isolated splitter.	2
Figure 1.2	Various common types of singly-fed circularly polarised patch elements....	5
Figure 1.3	An equivalent circuit of singly-fed circularly polarised square patch elements.....	6
Figure 1.4	Amplitude and phase diagrams for the single-layer SFCP microstrip patch elements [5, Ch 4].	6
Figure 1.5	Sanford’s multiple resonance radio frequency microstrip antenna structure in [21].	7
Figure 1.6	The six different configurations of EMC microstrip dipole introduced by Oltman in [26].	8
Figure 1.7	The two-layer stacked disc patch antenna reported in [23]. The top-patch is used as the driven patch.	8
Figure 1.8	The two-layer stacked disc patch antenna reported from [24]. The bottom patch is used as the driven patch.	8
Figure 1.9	A dual-frequency stacked patch antenna developed by Schaubert and Farrar [17].	9
Figure 1.10	Peter S. Hall <i>et al</i> proposed multilayer antennas using alumina substrates that allow for simple antenna and circuit integration in [25].	10

Figure 1.11 Sabban suggested the use of different dielectric constant (2.5 to 10.3) materials for the driven layer in [70]..... 11

Figure 1.12 The broadband multilayer patch antenna introduced by C. H. Chen *et al* in [71]. 11

Figure 1.13 A free-space dielectric layer introduced into the stacked patch antenna in [27]. 12

Figure 1.14 Dahele and Lee compared antenna performances arising from the different positions of the parasitic patch inside the stacked patch in [72]. 13

Figure 1.15 A proximity coupled patch antenna developed by D. Pozar in [34]..... 13

Figure 1.16 The high-performance probe-fed stacked patch antenna. A two-layer stacked patch antenna presented in [88]...... 13

Figure 1.17 The stacked patch antenna with a three-layer (sandwich) structure reported in [16], [78]. 14

Figure 1.18 The effect of superstrate on the performance of a CP-EMCP element: (a) Return Loss; and (b) Axial Ratio and Gain..... 15

Figure 1.19 The intrinsic axial-ratio (ABW) and impedance (ZBW) bandwidths of patch antennas as a function of total unloaded Q-factor..... 19

Figure 1.20 The relationship between axial ratio (AR)/standing wave ratio (SWR) and the cross-polarisation discrimination (XPD)/return loss (RL)..... 19

Figure 1.21 The axial ratio and gain measurement of a CP test antenna using the gain comparison method. 21

Figure 1.22 The receiving power of a 5.7 GHz *Type-E* element (AUT) using a linear spinning source. The measured axial ratio (dB) is the difference between the upper and lower envelopes. 23

Figure 1.23 A polarisation ellipse consisting the LH and RH components. 25

Figure 1.24 The two common types of polar radiation patterns: (a) peak and valley (max-min) power pattern, and (b) Power patterns with separated polarisation senses. 25

Figure 2.1 The transmission-line equivalent circuit for a LHCP cross-aperture coupled patch antenna. Two transformers with turn ratio of n_{1a} and n_{1b} model the coupling between the cross-aperture and the patch in the TM_{01} and TM_{10} mode, respectively; another transformer with turn ratio of n_2 models the coupling from the microstrip feedline to the cross-aperture. 31

Figure 2.2 (a) Axial ratio versus amplitude ratio ($|V_b|/|V_a|$) when phase error is $\pm 10^\circ$; (b) axial ratio versus phase error when $|V_b|/|V_a| = 1.19$; (c) axial ratio in dB as a function of both the phase error and the amplitude ratio of V_b and V_a35

Figure 2.3 The 2.4 GHz Cross-Aperture Coupled Patch (XACP) Antenna Structure (Type-F Element) with the use of stacked patches and tuning stub..... 37

Figure 2.4 The perturbation amount of stacked patches for the *Type-F* element is determined falling in the range of 6.072% to 7.175% of the squared patches. The perturbation curve for the *Type-A* element is included for comparison. 43

Figure 2.5 A design logic flow-chart for the 2.4 GHz *Type-F* element. 44

Figure 2.6 (a) Top view and (b) bottom view of the 2.4 GHz singly-fed cross-aperture coupled patch antenna (*Type-F* element) 45

Figure 2.7 Simulated and measured impedance locus with and without a $0.1\lambda_t$ tuning stub. 46

Figure 2.8 Simulated and measured CP gain and axial-ratio plots, with and without the $0.1\lambda_t$ shunt stub. 46

Figure 2.9 The measured co- and cross-polar radiation patterns at 2.36 GHz in two orthogonal planes: (a) x - z plane and (b) y - z plane..... 48

Figure 2.10 VSWR versus frequency as a function of upper-patch size, $P_2 = (a_2 \times b_2)$ 50

Figure 2.11 CP Gain versus frequency as a function of upper-patch size, $P_2 = (a_2 \times b_2)$ 50

Figure 2.12 Axial ratio versus frequency as a function of upper-patch size, $P_2 = (a_2 \times b_2)$ 51

Figure 2.13 The effect of Aperture Width (W_{xs}) and Length (L_{xs}) on Front-to-Back Lobe Ratio. 52

Figure 2.14 CP Gain versus Aperture Length (L_{xs}) and Width (W_{xs}) at two selected frequency points: 2.4 GHz and 2.5 GHz. 53

Figure 2.15 The minimum achievable axial-ratio versus Aperture Width (W_{xs}) and Length (L_{xs}). 53

Figure 3.1 Geometry of the right-hand circularly polarised EMCP antenna: (a) 3-D View; and (b) Side View 58

Figure 3.2 Patch-to-line width ratio and 50Ω line width as a function of both frequency and substrate thickness. Only four available thicknesses from RO3010™ at three frequencies are considered. 61

Figure 3.3 Stacked patches and its design variables for a RHCP-EMCP antenna (*Type-E* element). 62

Figure 3.4 A flowchart describing the design logic and tuning strategy. 65

Figure 3.5 Calculated VSWR responses of the square patches with various middle-layer heights whilst the squared patches $P_1=8.4\text{mm}$ and $P_2=18\text{mm}$ 69

Figure 3.6 Axial Ratio versus frequency as a function of perturbation (q_2) as in the first ($N=1$) to the fourth ($N=4$) simulation, when $P_1 = 8.4\text{ mm}$ 70

Figure 3.7 Axial Ratio as a function of perturbation on the parasitic patch (q_2) in the simulation $N=5$ to 7 , when $P_1=8.6\text{mm}$ and $d_2 = 3\text{mm}$ 71

Figure 3.8 Axial Ratio as a function of airgap length (d_2) when $P_1=8.6\text{mm}$, $P_2=18\text{ mm}$, $q_1=2.9$ and $q_2=4.6\text{ mm}$ 71

Figure 3.9 The CP Gain responses to airgap length (d_2) from 2.8 to 3.6 mm , when $P_1 = 8.6\text{ mm}$, $P_2 = 18\text{ mm}$, $q_1 = 2.9$ and $q_2 = 4.6\text{ mm}$ 72

Figure 3.10 The 3-dB Axial-Ratio Bandwidth and Minimum Axial-Ratio as a function of airgap length (d_2). 73

Figure 3.11 Simulated VSWR with and without shunt-stub included into the feedline and the measured VSWR with shunt-stub. 74

Figure 3.12 Simulated and measured CP Gain and Axial-Ratio with adding of a small shunt-stub of 2.20mm 74

Figure 3.13 Measured radiation patterns of both CP senses in two orthogonal planes at the centre frequency. 75

Figure 3.14 The photographs of the 5.8-GHz Singly-Fed *Type-E* elements (CP-EMCP): (a) Elevation View, and (b) Stacked patches. The elements have the optimal design parameters: $P_1 = 8.6\text{ mm}$, $P_2 = 18\text{ mm}$, $q_1 = 2.9\text{ mm}$, $q_2 = 4.6\text{ mm}$ when airgap length (d_2) is 3.2 mm 76

Figure 3.15 The variation of axial-ratio due to the coarse change of perturbation (q_2) from 0 to 2.0 mm on the parasitic patch, with $P_1 = 3.5\text{ mm}$, $P_2 = 7.3\text{ mm}$, $q_1 = 1.3\text{ mm}$ and $d_2 = 1.30\text{ mm}$ 78

Figure 3.16 The variation of Axial-Ratio due to changes of parasitic patch size (P_2) from 7.3 down to 6.5 mm in 4 uniform steps. $P_1 = 3.5\text{ mm}$, $q_1 = 1.3\text{ mm}$ $d_2 = 1.3\text{ mm}$ and $q_2 = 1.0\text{ mm}$ 79

Figure 3.17 The variation of axial-ratio due to the small change of perturbation (q_2) on the parasitic patch when $P_1 = 3.5$, $P_2 = 6.6$, $q_1 = 1.30$ and $d_2 = 1.30$ mm.	80
Figure 3.18 The Gain and VSWR vs frequency when $P_1 = 3.50$, $P_2 = 6.60$, $q_1 = 1.30$, $q_2 = 0.66$, $d_2 = 1.30$ mm.	81
Figure 3.19 The radiation patterns of both senses in two orthogonal planes at the centre frequency. The boresight XPD is greater than 15 dB.	81
Figure 3.20 The measured return loss ($-S_{11}$) plots of the 2.4 GHz CP-EMCP element when the airgap length is 7.5, 8.5 and 10.1 mm, respectively.	83
Figure 3.21 The measured input impedance loci of the 2.4-GHz CP-EMCP element for three airgap lengths: $d_2 = 7.5$, 8.5 and 10.1 mm.	84
Figure 3.22 The simulated and measured axial-ratio and circular polarisation gains versus frequency with airgap length (d_2) of 8.5 mm.	84
Figure 3.23 The measured radiation patterns of both senses (LHCP and RHCP) at 2.40 GHz in (a) x - z plane, and (b) y - z plane.	85
Figure 3.24 The reduced scale plot of the right-hand CP patterns in two orthogonal planes. The HPBW is about 60° in both the planes.	85
Figure 3.25 The photographs of the 2.4-GHz CP-EMCP element: (a) Parasitic (Top) Patch, and (b) Driven (Bottom) Patch.	86
Figure 3.26 A typical maximum frequency of operation for Rogers Microwave Materials.	88
Figure 3.27 The geometry of the broadband stacked patch in EMCP structure: (a) LP design; and (b) CP design at the centre frequency of 10 GHz.	89
Figure 3.28 Simulated and measured Gain and VSWR for the LP-EMCP element as shown in Fig. 3.27(a).	90
Figure 3.29 Simulated and measured return loss of a single X-band RHCP-EMCP element, a modified <i>Type-E</i> element with square parasitic patch.	91
Figure 3.30 Simulated and measured gain and axial-ratio of a single X-band RHCP-EMCP element. The results show both normal aligned and rotated top-patch.	91
Figure 3.31 Elliptical patch printed on a single-layer grounded substrate with defined parameters.	92
Figure 3.32 The evolution of modified <i>Type-E</i> element at X-band. A circular disc is stacked onto top of a quasi-ellipse.	95

Figure 3.33 The geometry and dimensions of the modification 2. A right-hand CP patch element at X-band with a circular patch stacked onto top of a driven quasi-ellipse. 95

Figure 3.34 The antenna efficiency and VSWR versus frequency for the circular disc stacked onto a quasi-elliptical patch..... 96

Figure 3.35 The antenna gain and axial ratio versus frequency for the circular disc stacked onto a quasi-elliptical patch..... 96

Figure 4.1 The X-O map indicative of the displacement loci for the top-patch in the LHP. X: centre of top-patch; O: the rotation of top-patch is taking place.102

Figure 4.2 Pictures show two specific displacements (a)a linear displacement at 4, 135°; and (b) the combination of linear and angular displacement of 45° at 4, 270°. 103

Figure 4.3 Measured S_{11} in dB for linear displacement in *five* directions: (a) 90°, (b) 135°, (c) 180°, (d) 225° and (e) 270° movement. Each plot shows the comparison of S_{11} for 2, 4, 6 mm with the normal alignment 0 0°. 105

Figure 4.4 Measured S_{11} in dB for angular displacement at *two* locations: (a) the origin 0 \angle 0°, (b) 4 \angle 270°. Each plot contains a comparison with the S_{11} for the perfectly aligned patch (0 \angle 0°)..... 106

Figure 4.5 The loci of displacement for the top-patch in the LHP. X denotes the locations where centres of top-patch were moved; and Δ denotes where the axial-ratio measurement were taken..... 109

Figure 4.6 Photographs of both the top (left hand side) and bottom (right hand side) layer of the X-band CP-EMCP antenna element before assembly of the stacked patches. 110

Figure 4.7 The measured return-loss plots for the 2-mm displacements in *3 directions* (90°, 180° and 270°), and compared to the simulated and measured results under normal alignment. 110

Figure 4.8 The measured return-loss plots for the 4-mm displacements in *5 directions* (90°, 135°, 180°, 225° and 270°), compared to the normal alignment. 111

Figure 4.9 The measured return-loss plots for the 6-mm displacements in *5 directions* (90°, 135°, 180°, 225° and 270°), compared to the normal alignment. 111

Figure 4.10 The measured axial ratio vs. frequency for the 2-mm displacements in *3 directions* (90°, 180° and 270°), compared to the normal alignment..... 112

Figure 4.11 The measured axial ratio vs. frequency for the 4-mm displacements in 5 directions (90° , 135° , 180° , 225° and 270°), and compared to the normal alignment. 112

Figure 4.11a The measured gain versus frequency as a function of 4-mm displacements in 5 directions, and compared to gain obtained from the normal alignment (0 , 0°). 114

Figure 4.12 The geometry of the stacked patch with CP-EMCP structure, where P_1 , P_2 , q_1 , and q_2 are the square patch length and the corresponding perturbation length of the stacked patches, respectively. 117

Figure 4.13 Return Loss plots of Design 1 for the angular displacement at the origin in five angles with the comparison to the normal alignment, 0° 118

Figure 4.14 Return-Loss plots of Design 2 for the angular displacement at the origin in three angles in (a) CCW and (b) CW directions with the comparison to the normal alignment, 0° 119

Figure 4.15 Gain and axial ratio plots of Design 1 for the angular displacement at the origin in three angles in both CCW and CW directions: (a) 10° , (b) 22° , and (c) 45° . Each plot has showed the comparison to the normal alignment, 0° 120

Figure 4.16 Gain and axial ratio plots of Design 2 for the angular displacement at the origin in three angles in both CCW and CW directions: (a) 10° , (b) 22° , and (c) 45° . Each plot shows the comparison to the normal alignment, 0° 121

Figure 4.17 The variation of VSWR for the C-band *Type-E* element due to thickness and dielectric constant tolerances on RO3010TM in four extreme-case scenarios. 124

Figure 4.18 The variation of CP gain for the C-band *Type-E* element due to thickness and dielectric constant tolerances on RO3010TM in four extreme-case scenarios. 125

Figure 4.19 The variation of axial ratio for the C-band *Type-E* element due to thickness and dielectric constant tolerances on RO3010TM in four extreme-case scenarios. 125

Figure 4.20 The variation of VSWR for the X-band modified *Type-E* element due to thickness and dielectric constant tolerances on RO3006TM in four extreme-case scenarios. 128

Figure 4.21 The variation of gain for the X-band modified *Type-E* element due to thickness and dielectric constant tolerances on RO3006TM in four extreme-case scenarios. 128

Figure 4.22 The variation of axial ratio for the X-band modified *Type-E* element due to thickness and dielectric constant tolerances on RO3006TM in four extreme-case scenarios. 129

Figure 4.23 The generic geometry in top-view of two rectangular patch elements in both the examinations..... 132

Figure 4.24 The computed E- and H-plane mutual coupling using EnsembleTM compared to the calculated and measured results by Mohammadian *et al* [95]. Single-layer patch antenna parameters: $a = 16$ mm, $b = 16.93$ mm, $x_o = 5.5$ mm, $y_o = 8$ mm, $t = 1.57$ mm, $\epsilon_r = 2.55$, $f_o = 5$ GHz. Note that d is the edge-to-edge distance between the elements. 133

Figure 4.25 The computed “E- and H-plane” mutual coupling versus edge spacing (d) using EnsembleTM compared to the calculated and measured results by Terret *et al* [97]. Stacked patch antenna parameters: $a_1 = b_1 = 40$ mm, $a_2 = b_2 = 43.2$ mm, $x_o = y_o = 18$ mm, $t_1 = t_3 = 1.6$ mm, $\epsilon_{r1} = \epsilon_{r2} = 2.19$, $\tan\delta_1 = \tan\delta_2 = 0.001$, $t_2 = 8.8$ mm, $\epsilon_{r2} = 1.0$, $f_m = 2.56$ GHz. Coaxial diameter: 1.27 mm..... 134

Figure 4.26 The definition of physical planes arrangement for a pair of CP-EMCP 1 in three orientations: (a) H-plane ($\varphi = 0^\circ$), (b) E-plane ($\varphi = 90^\circ$) and (c) D-plane ($\varphi = 45^\circ$). 136

Figure 4.27 (a) The E-plane and (b) H-plane mutual coupling of CP-EMCP elements versus centre-spacing (D) and compared to Antenna A1, A2, C1 and C2. 143

Figure 4.28 (a) The E-plane, (b) H-plane and (c) D-plane ($\varphi = 45^\circ$) mutual coupling of CP-EMCP elements versus centre-spacing and compared to Antenna B1, B2 and D..... 145

Figure 4.29 The return loss and the E-plane mutual coupling in frequency domain of a single patch antenna. The centre-spacings are 0.7, 1.1 and $1.7\lambda_o$. The antenna parameters: $a = 15.8$ mm, $b = 16.8$ mm, $x_o = 5.5$ mm, $y_o = 8$ mm, $t = 1.5$ mm, $\epsilon_r = 2.55$, $f_o = 5.22$ GHz. 146

Figure 4.30 The plots of return loss and mutual coupling of the stacked patch antenna having the *lo-lo-lo* dielectric-layers combination [107]. The maximum mutual coupling or mutual coupling at the centre frequency is varied with element spacing only..... 147

Figure 4.31 The mutual coupling curves and the S_{11} plots of CP-EMCP 1 for the 3 centre-spacings: $0.418\lambda_o$, $0.836\lambda_o$ and $1.6\lambda_o$ in (a) E-plane ($\varphi = 90^\circ$) and (b) H-plane ($\varphi = 0^\circ$). 148

Figure 4.32 The measured mutual coupling versus with frequency between two CP-EMCP2 elements in the orientations of (a) 90°-90°, (b) 270° - 90° 150

Figure 4.33 The mutual coupling between two CP-EMCP 1 elements versus with both the centre-spacing and the frequency in (a) Collinear plane ($\varphi = 90^\circ$), (b) Parallel plane ($\varphi = 0^\circ$). 151

Figure 4.34 (a) Collinear plane ($\varphi = 90^\circ$) and Parallel plane ($\varphi = 0^\circ$) mutual coupling between two CP-EMCP 2 elements for four superstrate thicknesses in spatial domain at 10 GHz. 154

Figure 4.35 The mutual coupling between two CP-EMCP 2 elements for *five* superstrate thicknesses in frequency domain at $D = 0.667\lambda_0$ in (a) Collinear plane ($\varphi = 0^\circ$) and (b) Parallel plane ($\varphi = 0^\circ$) 155

Figure 4.36 (a)The variation of return-loss for the CP-EMCP 2 element due to the change in superstrate thickness. (b) The effect of superstrate thickness on the CP characteristics of the CP-EMCP 2 element. 157

Figure 4.37 (a) The definition of orientation angles for a pair of CP stacked elements with an element spacing D . (b) The eight orientations of a single element with the associated E-field vectors in one competed cycle. 159

Figure 4.38 The mutual coupling at 10 GHz for the 64 β - α combinations of a pair CP-EMCP elements (antenna 1 and 2) when the element spacing is $2/3\lambda_0$ 161

Figure 4.39 (a) The 2-element RHCP-EMCP array oriented in the six β - α combinations: (A) 315°-45°, (B) 45°-315°, (C) 0°-180°, (D) 180°-0°, (E) 45°-45° and (F) 225°-0°. (b) The mutual coupling versus spacing at the centre frequency of 10 GHz for the six β - α combinations of a pair RHCP-EMCP elements... 163

Figure 4.40 (a)The four main orientation pairs of a two-element array: 270°-90° , 90°-90° (C-plane), 0°-0° (P-plane) and 90°-0° (O-plane). (b) The calculated compared to the measured mutual coupling versus spacing at the centre frequency of 10 GHz for the four main orientation pairs of RHCP-EMCP elements..... 164

Figure 4.41 A pair of 45°-oriented CP stacked patch antennas arranged at a constant spacing D with 9 orientations, $\Phi = [-90^\circ -67^\circ -45^\circ -22^\circ 0^\circ 22^\circ 45^\circ 90^\circ]$. 166

Figure 4.42 The mutual coupling between a pair of 45°-oriented CP stacked patch elements versus spcing D and orientation angle Φ at three frequencies: (a) 9.5 GHz, (b) 10.0 GHz and (c) 10.5 GHz. 167

Figure 5.1 Configuration of a sequential rotation array composed of singly-fed circularly polarised elements..... 175

Figure 5.2	Geometry of a 2x2 planar array composed of sequentially rotated singly-fed CP elements ($\#1 \sim \#4$) in a multiple of 90° <i>clockwise</i> ($p = 2$). The elements are arranged in a square grid and fed by the excitation voltages v_1 to v_4 according to the V_1 mode (RHCP).....	178
Figure 5.3	The cross-polarisation discrimination $XP D_f$ versus the quality factor δ of the feed network. The positive $XP D_f$ [dB] indicates a positive phase angle is required by δ for the generation of RHCP.	182
Figure 5.4	The eight radiation patterns at 10GHz from different configurations of the SRA as shown in Fig. 5.2. The RHCP elements are identical and fed by an ideal feed network with different rotations of spatial angle Φ_{sn} and excitation angle Φ_{en}	185
Figure 5.5	The conductor and dielectric losses of 50- Ω lines versus frequency in X-band. The microstrip lines are printed on the grounded material RO3010 and RO3006, respectively.	190
Figure 5.6	Radiation losses from three types of discontinuity on high-dielectric-constant materials RO3010 and RO3006: (a) Radiation loss on substrates of 0.635 mm versus frequency; (b) Radiation loss as a function of both substrate thickness and effective dielectric constant; (c) The total radiation losses from a feed network consists of 3 (IC+TJ)s and 10 RABs.....	192
Figure 5.7	The optimal chamfer of the four right-angle bends for the phase shifter. (a) The definition of the design parameters. (b) The variation of insertion loss at X-band for the 0 to 80% chamfered bends.	195
Figure 5.8	(a)Design of two-way power divider with a 45° phase offset (0° - 90° phase). (b)Design of the central stem composed of a 180° phase-shifter in the feed network. (c)A complete coplanar feed network for the 2x2 sequential rotation subarray.....	197
Figure 5.9	The (a) amplitude and (b) phase responses for the 4 output ports of the coplanar feed network as shown in Fig. 5.8(c)	199
Figure 5.10	The silhouette of 90° sequentially rotated 2x2 subarrays composed of the offset elements. (a) Array 1 has the square top-patches; (b) Array 2 has the circular top-patches.	200
Figure 5.11	Axial ratio and gain of Array 1 versus frequency. The simulated results compared with measured results.	201
Figure 5.12	Return Loss of Array 1: the simulated results compared with measured results.	202

Figure 5.13 Return Loss of Array 2: the simulated results compared with measured results.	202
Figure 5.14 The calculated directivity, gain and axial ratio of the array 2.	205
Figure 5.15 The calculated radiation efficiencies for the X-band single CP-EMCP elements and the 2x2 arrays.	205
Figure 5.16 Measured compared with simulated radiation patterns of Array 1 in $\phi = 0^\circ$ cut at (a) 9 GHz, (b) 10 GHz and (c) 11 GHz.	207
Figure 5.17 The measured radiation patterns compared with simulated results of Array 2 at 10 GHz. (a) $\phi = 0^\circ$ and (b) $\phi = 90^\circ$ cut.	208
Figure 5.18 Antenna measurement conducted inside the anechoic chamber at TIP, CSIRO.	209
Figure 5.19 A possible design of coplanar feed network for a 4x4 sequential rotation array. The rotation of excitation angle is <i>counter-clockwise</i>	210
Figure 5.20 The low loss coplanar feed network for a 4x4 sequential rotation array. The rotation of excitation angle is <i>clockwise</i>	211
Figure 5.21 The (a) amplitude and (b) phase responses of the SRA feed network as shown in Fig. 5.20.	212
Figure 5.22 The complete 4x4 sequential rotation array with a spacing of 20 mm in both the x- and y-directions. Both the spatial and excitation angles are CW directed.	213
Figure 5.23 The Gain, axial ratio and VSWR versus frequency for the 4x4 sequential rotation array as shown in Fig. 5.22.	215
Figure 5.24 The radiation patterns of LH and RHCP at 10 GHz in rectangular plot for the 4x4 sequential rotation array as shown in Fig. 5.22.	215
Figure 5.25 Radiation patterns in two principle planes ($\phi=0^\circ, 90^\circ$). (a) 8.9 GHz, (b) 9.5 GHz, (c) 10.5 GHz, (d) 11.0 GHz, (e) 11.5 GHz and (f) 11.8 GHz.	216
Figure 5.26 The antenna efficiency versus frequency for the 4x4 sequential rotation array comprises a low-loss feed network.	217
Figure A.1 The VSWR plot for the 4x4 sequentially rotated array as shown in Fig. 5.19.	245
Figure A.2 The CP gain and axial ratio versus frequency fro the 4x4 sequential rotated array as shown in Fig. 5.19.	246

List of Tables

Table 2.1	Summary of dielectric materials used for the <i>Type-F</i> Element.	36
Table 2.2	Summary of all design variables for the <i>Type-F</i> Element.	44
Table 2.3	Six parasitic/upper patch sizes	49
Table 3.1	Dielectric materials used for the 2.4-GHz <i>Type-E</i> element	82
Table 3.2	Summary of design variables for all <i>Type-E</i> elements	83
Table 3.3	Summary of bandwidths and mean frequencies obtained in 3 design examples	98
Table 4.1	Summary of 10-dB Impedance Bandwidths with Mean Frequencies for All Displacements.	107
Table 4.2	Linear Displacement Limits for the LP-EMCP element based on 10-dB ZBW Criterion of 10%.....	108
Table 4.3	Summary of 10-dB Impedance Bandwidths for Linear Displacements applied to CP-EMCP Element	113
Table 4.4	Summary of 3-dB Axial-Ratio Bandwidths for Linear Displacements applied to CP-EMCP Element	113
Table 4.5	Linear Displacement Limits for the CP-EMCP Element based on 3-dB ABW Criterion of 5%.....	115
Table 4.6	Summary of the Two X-band CP-EMCP Elements whose geometry is shown in Fig. 4.12.	116
Table 4.7	Angular Displacements (0° to $\pm 45^\circ$) on Two CP-EMCP Designs	117

Table 4.8 Summary of the substrate materials used in the Design Examples..... 123

Table 4.9 Summary of changes in impedance bandwidth and axial-ratio bandwidth in four extreme cases of tolerances on the substrate material RO3010TM 126

Table 4.10 Summary of changes in lowset axial ratio, impedance bandwidth and axial-ratio bandwidth for the four extreme cases of tolerances on the substrate material RO3006 127

Table 4.11 Design parameters of broadband CP-EMCP elements 136

Table 4.12(a) Summary of dielectric layers parameters of antennas having different architectures..... 138

Table 4.12(b) Stacked patches configurations and feeding methods of antenna elements in comparison 139

Table 5.1 Summary of design parameters for 2x2 feed network 198

Table 5.2 Summary of measured bandwidths for the 4-element subarrays203

Table 5.3 The amplitude, phase and errors of output ports at 9, 10 and 11 GHz213

List of Acronyms

ABC	Absorbing Boundary Condition
AR	Axial Ratio
ABW	Axial-Ratio Bandwidth
AUT	Antenna under Test
CF	Correction Factor
CP	Circular Polarisation
CP-EMCP	Circularly-polarised Electromagnetically Coupled Patch
CPG	Circular Polarisation Gain/Circular-gain
CW	Clockwise
CCW	Counter-Clockwise
EMCP	Electromagnetically Coupled Patch
EPA	Elliptical Patch Antenna
GBW	Gain Bandwidth
IC	Impedance Change
LHCP	Left-hand Circularly Polarised
LP	Linearly Polarisation
LPG	Linear Polarisation Gain/Linear-gain

OBW	Overlaid Bandwidth
RAB	Right-Angle Bend
RHCP	Right-hand Circularly Polarised
RL	Return Loss
RVWF	Rectangular Vector Wave Functions
SAR-RSW	Short Annular Ring-Reduced Surface-Wave antenna
SFCP	Singly-fed circularly polarised
SDA	Spectral Domain Approach
SGA	Standard Gain Antenna
SRA	Sequentially Rotated Array
SWR	Standing Wave Ratio
TJ	T-Junction
XACP	Cross-Aperture Coupled Patch antenna
XPD	Cross-polarisation Discrimination
ZBW	Impedance Bandwidth